# New electrodes for silver(II) electrogeneration: Comparison between Ti/Pt, Nb/Pt, and Nb/BDD

Ch. Racaud [a], A. Savall [a], Ph. Rondet [b], N. Bertrand [c], K. Groenen Serrano [a,*]

[a] Université de Toulouse, CNRS, INPT, UPS, Laboratoire de génie chimique, F-31062 Toulouse, France
[b] SGN, 25 Avenue de Tourville, 50120 Equerdreville, France
[c] AREVA NC, 1 Place Jean Millier, 92400 Courbevoie, France

## HIGHLIGHTS

- Nb/BDD electrode can efficiently generate silver(II) in nitric acid media.
- The comparison with Ti/Pt has shown that the generation rate was very similar.
- Simulation successfully predicted the behavior of the system.
- Competitive reactions with hydroxyl radical and Ag(II)/Ag(I) are negligible.

## GRAPHICAL ABSTRACT

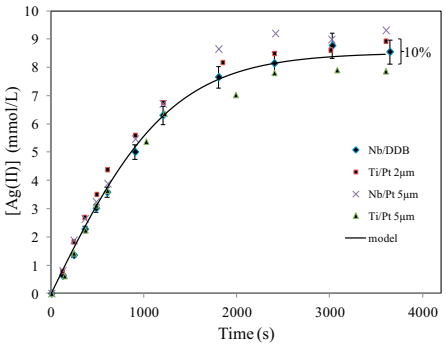


## ABSTRACT

Electrochemical processes based on the regeneration of silver(II) are very efficient for the destruction or dissolution of persistent substances. The aim of this work is to assess new anode materials to replace the conventional platinum electrode. The electrochemical generation of Ag(II) by oxidation of Ag(I) in $HNO_3$ (6 mol/L) was evaluated at boron doped diamond on niobium substrate (Nb/BDD) anode and results are compared with those obtained on Ti/Pt and Nb/Pt anodes. The performance of these anodes was evaluated in a filter press reactor in batch operation mode. The rate of Ag(II) generation obtained on the Nb/BDD anode is similar to that obtained on platinized electrodes. A theoretical model is presented to predict the behavior of the system. Good agreement is found between experimental results and the theoretical model.

*Keywords:*
Ag(II)
Boron doped diamond anode
Electrolysis
Electrosynthesis

## 1. Introduction

Processes involving mediated electrooxidation (MEO) have been extensively studied in the nuclear industry for the dissolution of contaminated materials or plutonium dioxide [1–5] and for the treatment of wastewater [6–9]. Among all electrogenerated oxidants, Ag(II) is one of the most convenient for such treatments, due to its high standard potential ($E^\circ$ = 1.98 V versus SHE). This species can be prepared by electrochemical oxidation of Ag(I) in concentrated nitric acid. The main advantages of this process are the working conditions: room temperature, atmospheric pressure, oxidant regeneration and recycling.

The kinetic process of silver(II) generation has been widely studied [4,5] on the platinum anode because of the good corrosion resistance and the electrocatalytic properties of this metal. The Ag(II) process implies several steps [5]: Ag(I) diffusion from the bulk to the anode surface, electron transfer and competitive reactions: water discharge and chemical reaction between Ag(II) and water [10–13]. The electrode activity being a key factor in the process, materials such as: glassy carbon, dimensionally stable anode

* Corresponding author.
*E-mail addresses:* philippe.rondet@areva.com (Ph. Rondet), nathalie.bertrand@areva.com (N. Bertrand), serrano@chimie.ups-tlse.fr (K. Groenen Serrano).

http://dx.doi.org/10.1016/j.cej.2012.09.010

(Ti/Pt, β-lead dioxide) and non-stoichiometric titanium oxide ceramic ($TiO_{2-x}$) have been investigated to find a substitute for the platinum [14]. The analysis of the rate constant of the oxidation of Ag(I), $k_{ox}$, reveals that the kinetics for all the materials were slower than for platinum with the $k_{ox}$ values three to four times lower. In potentiostatic conditions, the formation of a highly reactive solid, AgO, which precipitated at the anode due to the high local Ag(II) concentration was observed on glassy carbon and β-lead dioxide. Consequently, a deactivation of the electrode has occurred.

Boron doped diamond thin film electrodes (BDD) are known to have a wide potential window in aqueous solution, to be chemically inert in very aggressive media, and to show low adsorption properties and a strong resistance to deactivation [15,16]. BDD electrodes can act by direct electron transfer for potentials below that of water discharge or by indirect oxidation via electrogenerated hydroxyl radicals at high positive potentials in the region of water discharge [17]. Conducting diamond electrodes can be grown on various substrates such as silicon, titanium, niobium, tantalum, molybdenum and glassy carbon. For some industrial applications, niobium is chosen as substrate because of its mechanical robustness [18]. The electrochemical generation of Ag(II) on a Si/BDD anode has already been studied by Panizza et al. at the analytical scale in a conventional three-electrode cell [19]. In a previous study, cyclic voltammetry highlighted that a well-defined diffusion wave is obtained for the oxidation of 0.05 mol/L Ag(I) in 6 mol/L $HNO_3$ on a BDD anode [20]. Following these preliminary results, the aim of this paper is to study the electrochemical generation of Ag(II) in a two-compartment filter press reactor and to compare the performance of different anode materials: BDD on niobium substrate (Nb/BDD), titanium platinized with two different platinum thickness: 2 and 5 μm (Ti/Pt 2 μm and Ti/Pt 5 μm) and platinized niobium with 5 μm thick platinum (Nb/Pt 5 μm). A theoretical model taking into account the rates of Ag(II) electrochemical generation and the Ag(II) reduction by the water was developed and validated by experiments in the system developed.

## 2. Kinetic model

In the anodic compartment, $Ag^{2+}$ generated in aqueous nitric acid solution at 6 mol/L is stabilized by nitrate ion; thus in the absence of a reducing agent, most of the Ag(II) is present as a dark brown nitrate complex:

$$Ag + NO_3^- \xrightarrow{k_{II}} Ag(NO_3)^+ + e^- \quad (1)$$

However, the increase of the Ag(II) concentration induces a rise of the rate of water oxidation according to:

$$2Ag(NO_3)^+ + H_2O \rightarrow 2Ag^+ + 2HNO_3 + 0.5O_2 \quad (2)$$

Thus, the concentration of Ag(II) reaches a stationary value (resulting Eqs. (1) and (2)).

In the cathodic compartment, nitric acid is reduced to form nitrous acid.

$$HNO_3 + 2H^+ + 2e \rightarrow HNO_2 + H_2O \quad (3)$$

Referring to a batch recirculation reactor system, a modeling study was developed to simulate galvanostatic electrolysis. This model is based on mass balance in which the rate of Ag(II) generation is expressed as the difference between the production rate $R_{gen}$ by electrolysis and the destruction rate by reaction with water $R_{H_2O}$:

$$\frac{d[Ag(II)]}{dt} = R_{gen} - R_{H_2O} \quad (4)$$

The rate of Ag(II) production is given by:

$$R_{gen} = \frac{i_{Ag} S}{n F V_s} \quad (5)$$

where $i_{Ag}$ is the part of the current density used to generate Ag(II) ($A/m^2$), $S$ is the electrode surface area ($m^2$), $F$, the Faraday constant (96 485 C/mol), $n$, the number of electrons exchanged ($n = 1$) and $V_s$ the total volume of the solution ($m^3$); in a first approximation the volume of the electrochemical reactor is considered as small (63 mL) with regard to the total volume of solution (1 L).

$R_{H_2O}$ is the rate of Ag(II) hydrolysis; this redox reaction (Eq. (2)) has been well studied in nitric acid [10,11]. Its kinetic law involves Ag(II) and Ag(I) concentrations:

$$R_{H_2O} = k_{II} \frac{[Ag(II)]^2}{[Ag(I)]} \quad (6)$$

$k_{II}$ is the kinetic constant of Eq. (2)

The variation of Ag(II) concentration during electrolysis can be rewritten as follows:

$$\frac{d[Ag(II)]}{dt} = \frac{i_{Ag} S}{F V_s} - k_{II} \frac{[Ag(II)]^2}{[Ag(I)]} \quad (7)$$

Two different kinetic limitations are possible.

(i) *Kinetic regime under diffusion limitation*: when the applied current is higher than (or equals to) the initial limiting current, the partial current $I_{Ag}$ (A) is expressed using $k$ (m/s), the mass transfer coefficient:

$$I_{Ag} = I_{lim} = nFSk[Ag(I)] \quad (8)$$

In this case, the generation rate of Ag(II) is expressed by Eq. (9):

$$\frac{d[Ag(II)]}{dt} = \frac{k * S * [Ag(I)]}{V_s} - k_{II} \frac{[Ag(II)]^2}{[Ag(I)]} \quad (9)$$

When the applied current $I$ is much higher than the limiting current, $I_{lim}$, the rate of gas evolving at the electrode is enhanced. Vogt [21] proposed a correlation which defines a global mass transfer coefficient, $k_{global}$:

$$k_{global} = k_{bubbles} \left[ 1 + \left( \frac{k}{k_{bubbles}} \right)^2 \right]^{0.5} \quad (10)$$

$$k_{bubbles} = B \left( \frac{\dot{V}_g}{A} \right)^m D^{0.5} \quad (11)$$

where $k_{bubbles}$ depends on the gas flow production $\dot{V}_g$ ($m^3/s$), $D$ is the gas diffusion coefficient in the liquid phase ($m^2/s$), $B$ is a constant related to the bubbles (shape, diameter, surface tension); its value is estimated with experimental data results, $m$ is a function of the gas nature (in acidic media for oxygen, $m = 0.5$ [22–24]) and $A$ the area of the flow cross section ($m^2$).

$\left(\frac{\dot{V}_g}{A}\right)$ is a function of the applied current intensity which produces oxygen, $i_{O2}$ ($A/m^2$), and the molar volume of oxygen, $V_{mol}$ in $m^3$/mol (Eq. (12)):

$$\frac{\dot{V}_g}{A} = \frac{I_{O_2}}{nF} V_{mol} \quad (12)$$

(ii) *Kinetic regime under charge transfer limitation*: when the applied current, $I$, is lower than the limiting current throughout the transient period, the production rate $R_{gen}$ in Eq. (4) is simply expressed by:

$$R_{gen} = \frac{I}{F V_s} \quad (13)$$

The simulations were performed by numerically solving the mass conservation equations (Eqs. ((7), (9), and (13)) using a finite difference method [5]:

$$[\mathrm{Ag(II)}]_{t+\Delta t} = [\mathrm{Ag(II)}]_t + \Delta t\left(\frac{d[\mathrm{Ag(II)}]}{dt}\right)t \quad (14)$$

## 3. Materials and method

### 3.1. Electrochemical reactor

Electrolyses were performed under galvanostatic conditions in a two-compartment electrolytic flow cell (Diacell, Adamant Technologies, Switzerland) separated by a membrane (CMI-7000 Cation Exchange Membrane). All electrodes were disks with a working geometric area of 69 $cm^2$. Nb/BDD (Condias GmbH, Germany) [18], platinized titanium with two different platinum thicknesses (2 and 5 μm) and platinized niobium with 5 μm of platinum (Magneto special anodes B.V., Schiedam, The Netherlands) were used as anodes. The cathode was a Nb/BDD disk. The electrolytes were stored in two thermoregulated glass tanks (1 L capacity) and electrolyte recirculation was carried out using two peristaltic pumps. A sodium hydroxide gas scrubber was used to trap the $NO_x$ generated at the cathode. The flow rate in the electrochemical cell was 300 L/h. The range of the applied current intensity values was 0.1–5.3 A.

Current–potential curves for the Ag(II)/Ag(I) system were recorded under galvanostatic conditions in the Diacell reactor connected to a mercurous sulfate reference electrode (MSE, Hg/$Hg_2SO_4$/$K_2SO_4$).

### 3.2. Chemicals and analysis procedure

Silver nitrate ($AgNO_3$, Acros Organics, 99+%) was used for the electrogeneration of Ag(II). Nitric acid (VWR, analaR NORMAPUR, 68%) was used to prepare the electrolytic solutions.

Ag(II) was titrated by back potentiometry with Ce(III) (Acros Organics 99.5%) and Mohr's salt $(NH_4)_2Fe(SO_4)_2{\cdot}6H_2O$ (Acros Organics, 99+%). All the experiments were carried out with the optimal concentrations which were determined in a previous study [20]. The measurement of the generation rate of Ag(II) was standardized by considering the average variation of its concentration at the beginning of the electrolysis, which corresponds to the titration of three samples taken during the first 5 min. Values of the generation rate of Ag(II) were obtained by extrapolation to $t = 0$.

The kinetic constant $k_{II}$ was determined by assaying the Ag(II) concentration using UV spectroscopy ($\lambda$ = 580 nm, Hellma probe).

The conversion rate, X, of Ag(I) into Ag(II) is defined as the ratio of the silver(II) concentration to the initial Ag(I) concentration: $X = [\mathrm{Ag(II)}]/[\mathrm{Ag(I)}]_{initial}$.

The instantaneous current efficiency (ICE) at time t is defined by:

$$\mathrm{ICE} = \frac{[\mathrm{Ag(II)}]V_s F}{It}100 \quad (15)$$

Each experience was performed three times, the deviation does not exceed 5%, the average value is retained.

## 4. Results and discussion

### 4.1. Mass transport rate

Application areas of the Ag(II)/Ag(I) redox couple in the nuclear industry involve mass transport control; indeed the Ag(I) initial concentration is generally less than 0.1 mol/L in concentrated $HNO_3$. Thus, the limiting current is an important parameter for the characterization of mass transport rates in Ag(II) electrosynthesis. Under the limiting current conditions, the process operates at the maximum rate. In an electrochemical process the limiting current is defined as the value when the change of the current with potential is minimum or zero (i.e.; when $d(I)/d(E) = 0$) [25].

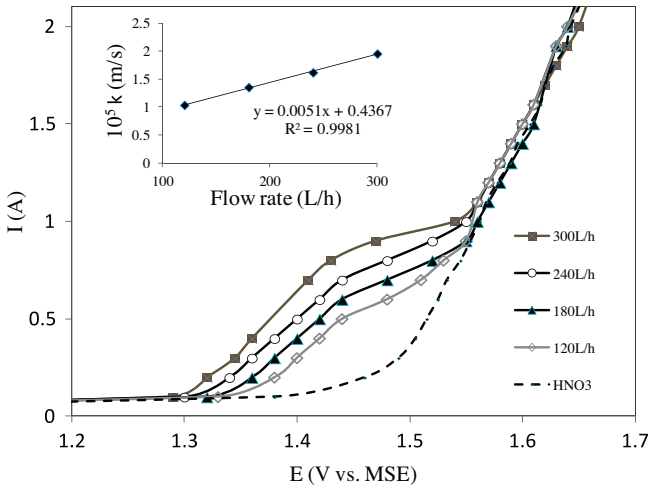


**Fig. 1.** *I* versus *E* curves at different flow rates using the filter press reactor with the Ti/Pt 5 μm anode, $[AgNO_3]$ = 0.05 mol/L in 6 mol/L $HNO_3$; $T$ = 30 °C. Inset panel: values of $k$ as a function of flow rate.

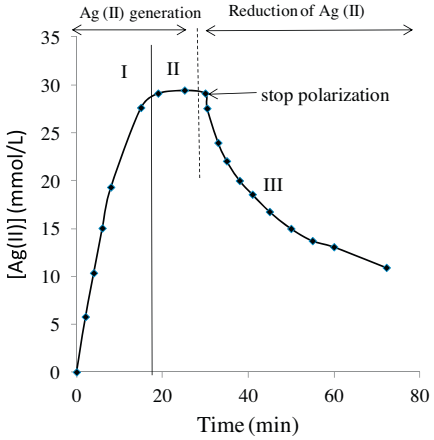


**Fig. 2.** Temporal variation of silver(II) concentration. ($[Ag(I)]$ = 0.1 mol/L; $[HNO_3]$ = 6 mol/L; $T$ = 25 °C; anode: Ti/Pt, flow rate: 300 L/h).

Fig. 1 shows plots of the oxidation process corresponding to Eq. (1) with $[Ag(I)]_{initial}$ = 0.05 1 mol/L in 1 L of 6 mol/L $HNO_3$. These curves were obtained under galvanostatic conditions at different flow rates for the DiaCell reactor. Each point was registered after 3 s at constant current. Each curve was plotted in direct and reverse scan; both scans gave the same result. During the drawing of a curve the decrease of the Ag(I) concentration was less than 1.5%. Ag(I) oxidation appears distinctly before water discharge; the oxidation wave of Ag(I) presents the classic shape of the progressive change of the kinetic limitation from charge transfer to mass transfer with increasing potential. The diffusion plateau reaches a 100 mV length. The mass transfer coefficient $k$ was then determined using the limiting current measured at 1.48 V and corrected taking into account the residual current $HNO_3$ (6M) (Eq. (8)).

In the operating range of flow rate (120–300 L/h), at 30 °C, the variation of $k$ is correctly represented by a linear variation of the form:

$$k \times 10^5(\mathrm{m/s}) = 0.0051ø(\mathrm{L/h}) + 0.4367 \quad (16)$$

For example, at the working flow rate (300 L/h), the mass transfer coefficient is equal to $1.96 \times 10^{-5}$ m/s.

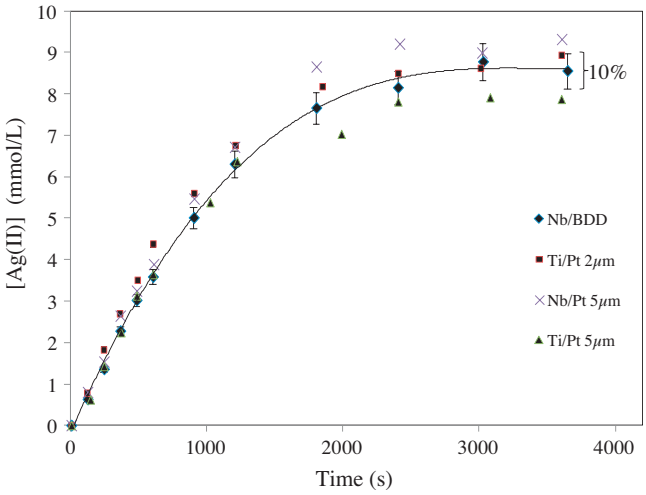


**Fig. 3.** Variation of Ag(II) concentration during electrolysis on different anode materials (Nb/BDD, Ti/Pt 2 µm, Ti/Pt 5 µm, Nb/Pt 5 µm). ($[AgNO_3]° = 0.05$ mol/L; $[HNO_3] = 6$ mol/L; $T = 30$ °C; $I = 1.1$ A; $I°_{lim} = 0.67$ A; flow rate: 300 L/h).

**Table 1**
Generation rate of silver II as a function of current for Nb/BDD, Ti/Pt 2 µm, Ti/Pt 5 µm, Nb/Pt 5 µm. ($[AgNO_3]° = 0.05$ mol/L, $[HNO_3] = 6$ mol/L, $I°_{lim} = 0.65$ A, $T = 30$ °C, flow rate: 300 L/h, $V_s = 1$ L).

| Applied current (A) | Generation rate (mol $m^{-2}$ $min^{-1}$) | | | |
|---|---|---|---|---|
| | Nb/BDD | Ti/Pt 2 µm | Ti/Pt 5 µm | Nb/Pt 5 µm |
| 0.1 | 0.006 | 0.006 | 0.008 | 0.008 |
| 0.5 | 0.032 | 0.036 | 0.043 | 0.039 |
| 1.1 | 0.053 | 0.066 | 0.054 | 0.061 |
| 2.5 | 0.062 | 0.074 | 0.074 | 0.074 |
| 3.5 | 0.080 | 0.078 | 0.080 | 0.086 |
| 5.3 | 0.091 | 0.083 | 0.103 | 0.100 |

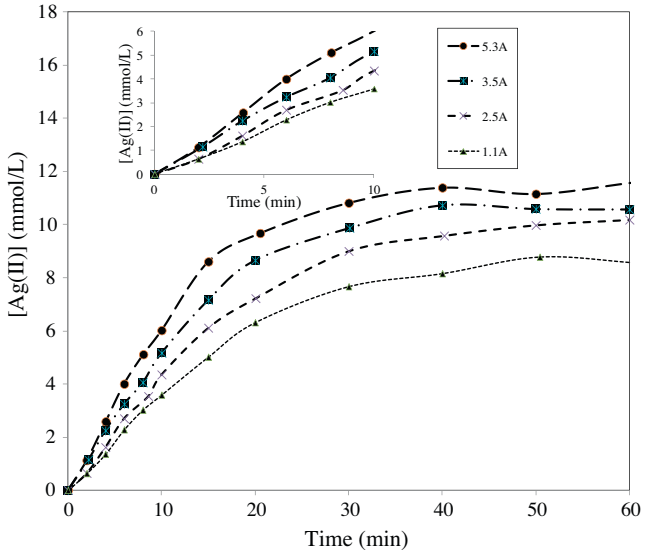


**Fig. 4.** Variation of Ag(II) concentration during electrolyses at different current intensities on Nb/BDD anode. ($[AgNO_3]° = 0.05$ mol/L; $[HNO_3] = 6$ mol/L, $T = 30$ °C, flow rate: 300 L/h, $I°_{lim} = 0.67$ A).

### 4.2. Measurement of the Ag(II) generation rate

Fig. 2 plots the Ag(II) concentration versus duration of electrolysis and after the interruption of polarization. Firstly, the concentration of Ag(II) increases with time (zone I) and then tends to a

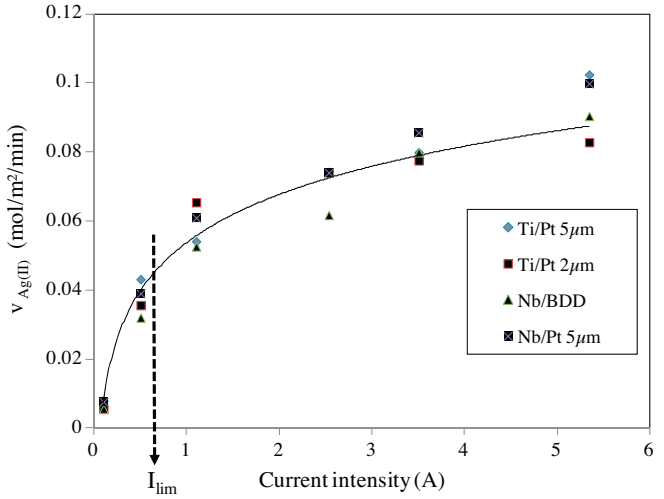


**Fig. 5.** Variation of Ag(II) generation rate at different current intensities on Ti/Pt 5 µm, Ti/Pt 2 µm, Nb/Pt 5 µm and Nb/BDD anode. ($[AgNO_3]° = 0.05$ mol/L; $[HNO_3] = 6$ mol/L; $T = 30$ °C; flow rate: 300 L/h; $I°_{lim} = 0.67$ A).

**Table 2**
Rate constants obtained at 25 °C by various authors ($[Ag(I)]° = 0.1$ mol/L, $[HNO_3] = 6$ mol/L).

| $k_{II}$ ($s^{-1}$) | Method | References |
|---|---|---|
| $7.9 \times 10^{-4}$ | Chemical | Arnaud et al. [14] |
| $7.6 \times 10^{-4}$ | Chemical | Noyes et al. [11] |
| $8.2 \times 10^{-4}$ | UV spec. | Po et al. [10] |
| $7.4 \times 10^{-4}$ | Potentiometry | Lehmani et al. [12] |
| $9.5 \times 10^{-4}$ | UV spec. | This study |

stationary value (zone II). This plateau corresponds to the balance between the electrochemical rate of Ag(II) generation and the chemical rate of its reduction by water according to Eq. (2).

After the interruption of electrolysis, the Ag(II) concentration decreases with time due to its reduction by water (Eq. (2)) (zone III).

Because of the increasing effect of the chemical reduction of Ag(II) (Eq. (2)) during the first phase, the electrochemical generation rate was determined for the different electrode materials at the beginning of the electrolysis of a solution. In addition, we made a more detailed study of the behavior of electrodes for applied currents $I$ higher than the initial limiting current of Ag(I) oxidation in order to estimate their performance under conditions close to those used in industry.

Fig. 3 shows the variation of Ag(II) concentration during electrolysis using different anode materials: Nb/BBD, Ti/Pt (2 µm and 5 µm) and Nb/Pt (5 µm). This figure shows that for Ag(II) = 0.05 - mol/L, the maximum conversion rate, $X$, is around 17.5% at 30 °C on Nb/BDD while it is slightly higher on Nb/Pt (18.6%). The Ag(II) generation rate seems similar for the different anodes.

More accurately, Table 1 summarizes the values of the Ag(II) generation rate extrapolated to $t = 0$ obtained for each anode. Assuming that the hydrodynamic conditions are similar for all the anodic materials tested, one can conclude that the rates obtained on the Nb/BBD electrode are slightly lower as that observed on Ti/Pt and Nb/Pt electrodes. This slight difference could result from morphological differences between electrodes. Indeed, the measured roughness of Nb/Pt is 30% higher than Nb/BDD (2276 nm), which could explain a higher active surface of the platinized electrode. Moreover, these results confirm that the thickness of platinum has no influence on the generation rate of Ag(II).

Fig. 4 shows the Ag(II) concentration variation during electrolyses carried out under galvanostatic conditions at different current densities in the case of the Nb/BDD anode. The influence of the

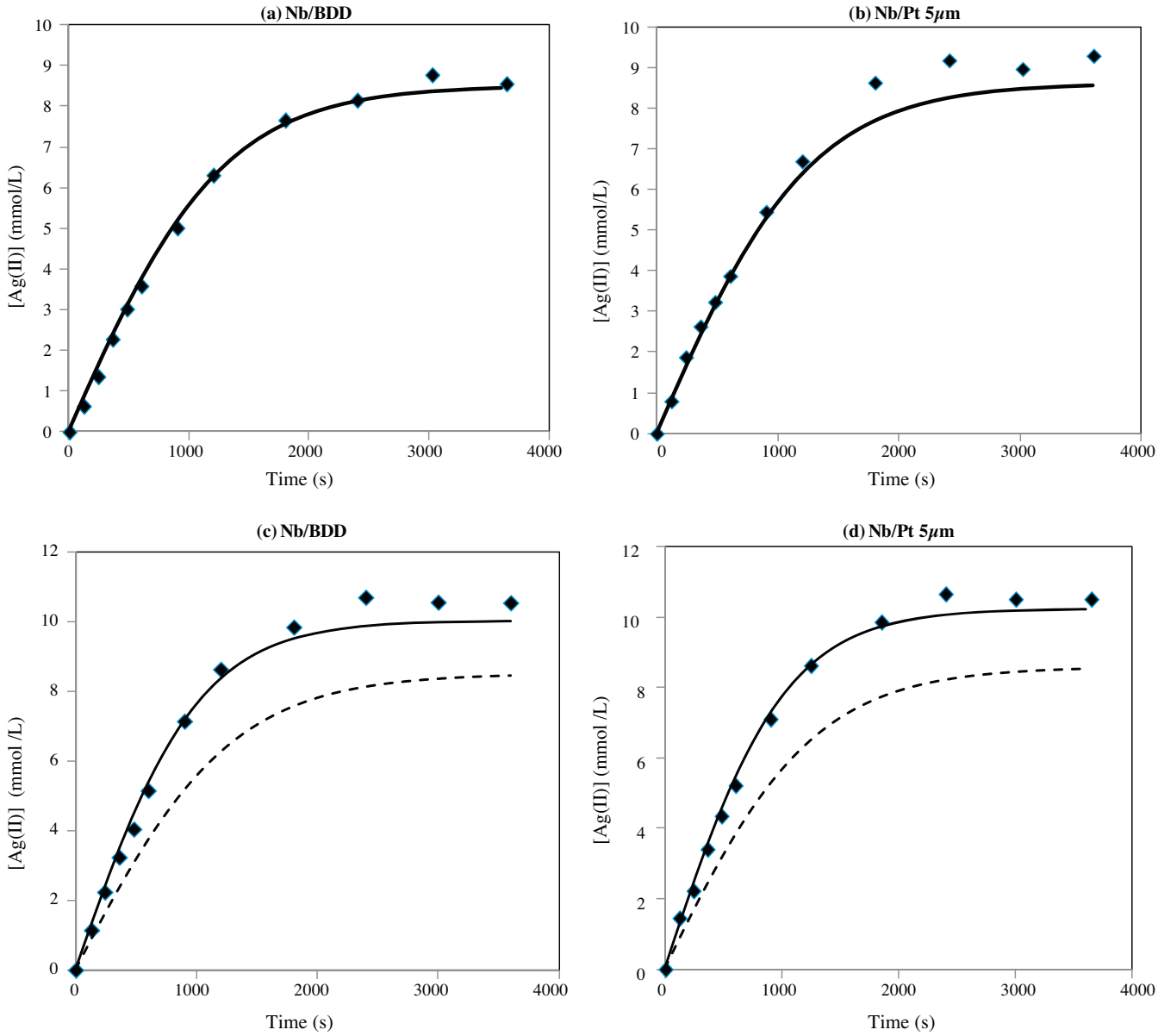


**Fig. 6.** Calculated (line) and experimental (symbol) of [Ag(II)] = $f(t)$ curves on (a) Nb/BDD and (b) Nb/Pt 5 μm at $I$ = 1.1 A and on (c) Nb/BDD and (d) Nb/Pt 5 μm at $I$ = 3.5A (continuous line: modelling using $k_{global}$, dotted line: modelling using k (Eq.(16)). ([$AgNO_3$] = 0.05 mol/L in 6 mol/L $HNO_3$, $k = 1.96 \times 10^{-5}$ m/s, $k_{II} = 1.64 \times 10^{-3}$ $s^{-1}$, $T$ = 30 °C, flow rate: 300 L/h;).

current density on the Ag(II) generation rate for different anodes under conditions for which $I_{lim}$ = 0.67 A is shown in Fig. 5.

These curves show that the higher the current density, the greater the initial generation rate.

As expected for $I < I_{lim}$ (Eq. (13)), the generation rate increases with $I$, whereas above $I_{lim}$, this rate increases more slowly. Eq. (9) cannot explain why the Ag(II) generation rate increases with the current density. However, it can be taken into account that during electrolysis, the depletion of Ag(I) leads to an increasing part of the current using for water discharge; a higher production of oxygen bubbles occurs. As shown in Eq. (10), the mass transfer coefficient increases locally.

### 4.3. Theoretical model of Ag(II) electrogeneration

The simulation results were carried out at currents higher ($I$ = 1.1 A and $I$ = 3.5 A) than the initial limiting current ($I^{\circ}_{lim}$ = 0.65 A). The results obtained were compared with experimental data obtained for electrolysis under galvanostatic conditions. To perform the simulation, besides the mass transfer coefficient, the kinetic constant of Eq. (2) must be known.

**Table 3**
Mass transfer coefficient due to gas evolution ($k_{bubbles}$) and global mass transfer coefficient ($k_{global}$) using the Vogt correlation ([Ag(I)]° = 0.05 mol/L, [$HNO_3$] = 6 mol/L, $T$ = 30 °C, $I$ = 3.5 A, $k = 1.96 \times 10^{-5}$ m $s^{-1}$).

| Electrode materials | $B^* D^{0.5}$ | $10^5 \times k_{global}$ (m/s) | $10^5 \times k_{bubbles}$ (m/s) |
|---|---|---|---|
| Nb/DDB | $4.3 \times 10^{-3}$ | 2.9 | 2.2 |
| Nb/Pt 5 μm | $4.2 \times 10^{-3}$ | 2.9 | 2.2 |
| Ti/Pt 2 μm | $2.4 \times 10^{-3}$ | 2.3 | 1.2 |
| Ti/Pt 5 μm | $2.5 \times 10^{-3}$ | 2.3 | 1.3 |

#### 4.3.1. Experimental determination of the kinetic constant $k_{II}$ of the oxidation of water by Ag(II)

Galvanostatic electrolyses were carried out at 25 °C and [Ag(I)]° = 0.05 mol/L on Ti/Pt and Nb/BDD anodes in the set-up.

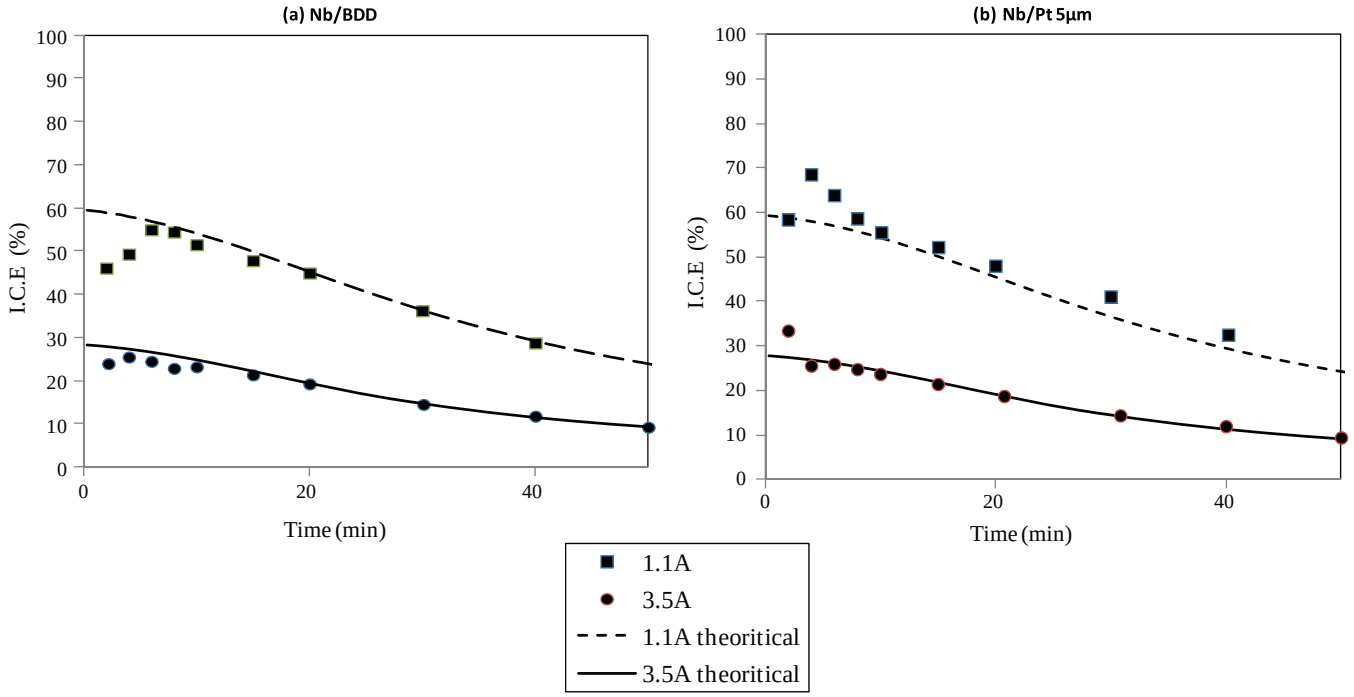


**Fig. 7.** Variation of the instantaneous current efficiency during electrolysis at two different currents on (a) Nb/BDD anode and (b) Nb/Pt 2 µm ([AgNO3] = 0.05 mol/L; [HNO3] = 6 mol/L, $T$ = 30 °C, $I^{\circ}_{lim}$ = 0.67 A; flow rate: 300 L/ h).

When a steady state was reached for the Ag(II) concentration, electrolysis was stopped and the Ag(II) concentration monitored versus time to measure the rate of Ag(II) reduction (Fig. 2). Then $k_{II}$ was determined from Eq. (6). The activation energy was calculated for this reaction between 20 and 35 °C; the value obtained 97.2 kJ/mol is in agreement with that obtained by different authors [10,11]. Table 2 presents the values of constant $k_{II}$ obtained in this study as well as some values available in the literature.

*4.3.2. Comparison of theory and experiment*

The comparison was made for two different values of initial currents: (i) higher than the limiting current (1.1 A) and (ii) much higher than the limiting current (3.5 A).

(i) simulation at $I$ = 1.1 A $(I/I^{\circ}_{lim} = 1.7)$

Fig. 6a and b shows the simulation according to Eq. (9) and the experimental values obtained during electrolyses on Nb/BDD and on Nb/Pt 5 µm. In this model, only the production rate by electrolysis and the rate of Ag(II) hydrolysis are taken into account and it is seen that the model predicts the data fairly well. But, at a current higher than the limiting current we can expect competitive reactions between hydroxyl radicals and silver species [26,27] according to Eqs. (17)–(21).

$$H_2O \rightarrow {\cdot}OH + H^+ + e^- \quad (17)$$

$$Ag^+ + {\cdot}OH \rightarrow AgO + H^+ \quad (18)$$

The insoluble compound formed AgO decomposes to give Ag(I) according to the following equation:

$$AgO + H^+ \rightarrow Ag^+ + 1/2H_2O + 1/4O_2 \quad (19)$$

Another competitive reaction may be suggested; an increasing current density enhances hydrogen peroxide formation (Eq. (20), $k_{20}$ = 5.5 × $10^9$ L $mol^{-1}$ $s^{-1}$ [28]) which causes the reduction of Ag(II) close to the electrode surface (Eq. (21), $k_{21}$ = 300 $s^{-1}$ [13]).

$${\cdot}OH + {\cdot}OH \overset{k_{20}}{\rightarrow} H_2O_2 \quad (20)$$

$$2Ag(NO_3)^+ + H_2O_2 \overset{k_{21}}{\rightarrow} 2Ag^+ + O_2 + 2H^+ + 2NO_3^- \quad (21)$$

The good agreement between experiment and simulation proves that competitive reactions are not present or even can be neglected as can the hydrodynamic effect of gas evolution.

(ii) simulation at $I$ = 3.5 A $(I/I^{\circ}_{lim} = 5.4)$

Fig. 6c and d shows that for a current intensity much higher than the limiting current, the experimental values of the Ag(II) concentration are higher than those calculated from the model (Eq. (9)). When the applied current $I$ is much higher than the limiting current, $I_{lim}$, the rate of gas evolving at the electrode is enhanced. The mass transfer coefficient of Eq. (10) was estimated for each material from experimental data acquired during electrolysis conducted at currents higher than the limiting current. Table 3 summarizes the mass transfer contribution due to gas evolution, $k_{bubbles}$, and the global mass transfer coefficient, $k_{global}$, according to the correlation of Vogt Eqs. (10)–(12). Taking this corrected $k_{global}$ value, the theoretical curve (continuous line) shows excellent fitting with the experimental points as can be seen in Fig. 6c and d.

Fig. 7 shows the variation of the experimental and theoretical instantaneous current efficiency (ICE) obtained at two currents (1.1 A and 3.5 A) on Nb/BDD and Ti/Pt 2 µm anodes. The theoretical ICE is calculated with the theoretical Ag(II) obtained in Fig. 6.

Note that, except for at the beginning of electrolysis ($t$ < 6 min), the theoretical value decays show an excellent fit with the experimental points whatever the applied current and the anode material. The very similar values obtained confirm that competitive reactions with hydroxyl radicals which can occur with a BDD anode are in fact negligible.

The difference between the first three experimental points and the model for both electrodes can be explained by the experimental

error of the Ag(II) titration owing to the very low concentration of Ag(II) at the start of electrolysis. Moreover, stationary hydrodynamic conditions are not reached at the beginning of electrolysis.

## 5. Conclusion

It has been shown that the Nb/BDD electrode can efficiently generate Ag(II) in nitric acid media. Compared to results found with platinized electrodes (Ti/Pt 2 and 5 μm and Nb/Pt 5 μm) the generation rate was very similar and the conversion rate was of the same order of magnitude. Contrary to bibliography [14], no deactivation of electrodes was observed. Simulation successfully predicted the behavior of the system. The theoretical results were compared with experimental data and the good agreement found indicates that competitive reactions with hydroxyl radical and Ag(II)/Ag(I) can be ignored.

For industrial applications, the choice of the anode will be confirmed after evaluation of the service life of each material under typical conditions of electrolysis. This study is in progress.

## References


[1] J.L. Ryan, L.A. Bray, Dissolution of plutonium dioxide – a critical review, actinides separations. Navratil JD, WW Schulz (Eds.), ACS Symp. Ser. 117 (1980) 499–514.

[2] J. Bourges, C. Madic, G. Koehly, M. Lecomte, Dissolution du bioxyde de plutonium en milieu nitrique par l'argent(II) electrogénéré, J. Less-Comm. Met. 122 (1986) 303–311.

[3] M. Lecomte, J. Bourges, C. Madic, Applications du procédé de dissolution oxydante du bioxyde de plutonium, in: Proc. Recod'87: International Conference on Nuclear Fuel Reprocessing and Waste Management, France, 23 August, 1987.

[4] Y. Zundelevich, The mediated electrochemical dissolution of plutonium oxide: kinetics and mechanism, J. Alloys Compd. 182 (1992) 115–130.

[5] Z. Chiba, C. Dease, Modeling of a Dissolution System for Transuranic Compounds, Report no. W-7405-ENG-48, Laurence Livermore National Laboratory, US, April, 1993.

[6] D.F. Steele, D. Richardson, D.R. Craig, J.D. Quin, P. Page, Destruction of industrial organic wastes using electrochemical oxidation, Plat. Met. Rev. 34 (1990) 10–14.

[7] M. Fleishmann, D. Pletcher, A. Rafinski, The kinetics of the silver(I)/silver(II) couple at a platinum electrode in perchloric and nitric acids, J. Appl. Electrochem. 1 (1971) 1–7.

[8] K. Chandrasekara Pillai, S.J. Chung, I.S. Moon, Studies on electrochemical recovery of silver from simulated waste water from Ag(I)/Ag(II) based mediated electrochemical oxidation process, Chemosphere 73 (2008) 1505–1511.

[9] E. Mentasti, C. Baiocchi, J.S. Coe, Mechanistic aspects of reactions involving Ag(II) as an oxidant, Coord. Chem. Rev. 54 (1984) 131–157.

[10] H.N. Po, J.H. Swinehart, T.L. Allen, The kinetics and mechanism of the oxidation of water by Ag(II) in concentrated nitric acid solution, Inorg. Chem. 7 (1968) 244–249.

[11] A.A. Noyes, J.L. Hoard, K.S. Pitzer, Argentic salts in acid solution – Part IV: The kinetics of the reduction by water and the formation by ozone of argentic silver in nitric acid solution, J. Am. Chem. Soc. 59 (1937) 1316–1325.

[12] A. Lehmani, P. Turq, J.P. Simonin, Oxidation of water and organic compounds by silver(II) using a potentiometric method, J. Electrochem. Soc. 143 (1996) 1860–1865.

[13] P.J.W. Rance, G.P. Nikitina, V.A. Korolev, M.Yu. Kirshin, A.A. Listopadov, V.P. Egorova, Features of electrolysis of nitric acid solutions of silver I. Behavior of Ag(II) in $HNO_3$ solutions, Radiochemistry 45 (2003) 346–352.

[14] O. Arnaud, C. Eysseric, A. Savall, Optimising the anode material for electrogeneration of Ag(II), Inst. Chem. Eng. Symp. Ser. 145 (1999) 229–238.

[15] J.J. Carey, C.S. Christ, S.N. Lowery, Electrolysis of Liquid Wastes Using a Doped Diamond Anode to Oxidize Solutes, US Patent 5399247, 1995.

[16] M. Panizza, G. Cerisola, Application of diamond electrodes to electrochemical processes, Electrochim. Acta 51 (2005) 191–199.

[17] D. Gandini, P.A. Michaud, I. Duo, E. Mahé, W. Haenni, A. Perret, Ch. Comminellis, Electrochemical behavior of synthetic boron-doped diamond thin films anodes, New Diam. Front. Carb. Technol. 9 (1999) 303–316.

[18] M. Fryda, Th. Matthée, S. Mulcahy, A. Hampel, L. Schafer, I. Troster, Fabrication and application of Diachem electrodes, Diam. Rel. Mater. 12 (2003) 1950–1956.

[19] M. Panizza, I. Duo, P.A. Michaud, G. Cerisola, Ch. Comminellis, Electrochemical generation of silver(II) at boron-doped diamond electrodes, Electrochem. Solid-State Lett. 3 (2000) 550–551.

[20] C. Racaud, K. Groenen-Serrano, A. Savall, Ph. Rondet, N. Bertrand, Recent advances in the electrochemical regeneration of Ag(II), in: Proceed. 9th Europ. Symp. on Electrochemistry, Chania, 2011, pp. 41–50.

[21] H. Vogt, Mass transfer at gas involving electrodes with superposition of hydrodynamic flow, Electrochim. Acta 23 (1978) 203–205.

[22] T.R. Beck, A contribution to the theory of electrolytic chlorate formation, J. Electrochem. Soc. 116 (1969) 1038–1041.

[23] L.J.J. Janssen, J.G. Hoogland, The effect of electrolytically evolved gas bubbles on the thickness of the diffusion layer, Electrochim. Acta 15 (1970) 1013–1023.

[24] L.J.J. Janssen, J.G. Hoogland, The effect of electrolytically evolved gas bubbles on the thickness of the diffusion layer II, Electrochim. Acta 18 (1973) 543–550.

[25] C. Ponce-de-Léon, C.T.J. Low, G. Kear, F.C. Walsh, Strategies for the determination of the convective diffusion limiting current from steady state linear sweep voltammetry, J. Appl. Electrochem. 37 (2007) 1261–1270.

[26] P.C. Beaumont, E.L. Powers, Radiation sensitivity of DNA–metal complexes: a pulse radiolysis study, Int. J. Radiat. Biol. Relat. Stud. Phys. Chem. Med. 43 (1983) 485–494.

[27] M. Bonifacic, Ch. Schoneich, K.-D. Asmus, Halogenated peroxyl radicals as multi-electron oxidants: pulse radiolysis study on the reaction of trichloromethyl peroxyl radicals with iodide, J. Chem. Soc. Chem. Commun. 23 (1991) 1117–1119.

[28] G.V. Buxton, C.L. Greenstock, W.P. Helman, A.B. Ross, Critical review of rate constants for reactions of hydrated electrons, hydrogen atoms and hydroxyl radicals, ($OH$, $O2^-$) in aqueous solution, J. Phys. Chem. Ref. Data 17 (1988) 513–886.